8578 *Inorg. Chem.* **2010**, *49*, 8578–8582
DOI: 10.1021/ic101180h

Inorganic Chemistry
Article

Synthesis and Characterization of the Crystal Structure and Magnetic Properties of the Ternary Manganese Vanadate $NaMnVO_4$

Hamdi Ben Yahia,*,† Etienne Gaudin,† Khalid Boulahya,‡ Jacques Darriet,† Won-Joon Son,§ and Myung-Hwan Whangbo§

†*ICMCB, CNRS, Université Bordeaux 1, 87 Avenue du Docteur Schweitzer, 33608 Pessac Cedex, France,* ‡*Departamento de Química Inorgánica Facultad de Químicas Universidad Complutense, 28040 Madrid, Spain, and* §*Department of Chemistry, North Carolina State University, Raleigh, North Carolina 27695-8204, USA*

Received June 11, 2010

A new ternary manganese vanadate, $NaMnVO_4$, was synthesized by solid state reaction route, and its crystal structure and magnetic properties were characterized by X-ray diffraction, magnetic susceptibility and specific heat measurements, and by density functional calculations. $NaMnVO_4$ crystallizes in the maricite-type structure with space group *Pnma*, $a = 9.563(1)$ Å, $b = 6.882(1)$ Å, $c = 5.316(1)$ Å, and $Z = 4$. $NaMnVO_4$ contains MnO_4 chains made up of edge-sharing MnO_6 octahedra, and these chains are interlinked by VO_4 tetrahedra. The magnetic susceptibility has a broad maximum at $T_{max} = 24$ K and follows the Curie−Weiss behavior above 70 K with $\theta = -62$ K. $NaMnVO_4$ undergoes a three-dimensional antiferromagnetic ordering at $T_N = 11.8$ K. The spin exchanges of $NaMnVO_4$ are dominated by the intrachain antiferromagnetic exchange, and the interchain spin exchanges are spin-frustrated. The most probable magnetic structure of the ordered magnetic state below T_N was predicted on the basis of the extracted spin exchanges.

1. Introduction

Many phosphates with the general formula $ABPO_4$ (A = alkali, Cu, Ag; B = transition metal) crystallize mainly in four different structural types, i.e., olivine, maricite, stuffed-tridymite, and zeolite-ABW. The stuffed-tridymite and zeolite-ABW structure types are observed with large alkali metals such as K, Rb, and Cs. In these structures, the transition metal is found mainly at tetrahedral sites and sometimes at trigonal bipyramidal sites. In the more condensed phases with olivine and maricite-type structures, the transition metal is located at an octahedral site. It is of interest to compare the structural evolution between homologous phosphates and vanadates, AMnPO$_4$ and AMnVO$_4$, respectively. In the AMnPO$_4$ phosphates series, LiMnPO$_4$,[1] NaMnPO$_4$,[2] KMnPO$_4$,[3] and CsMnPO$_4$[4] were studied in the past and their structures determined. Recently, we reported the structural and magnetic properties of RbMnPO$_4$[5] and AgMnPO$_4$.[6] In the homologous AMnVO$_4$ vanadates, LiMnVO$_4$[7] is known to crystallize in the Na_2CrO_4-type structure. In contrast to the case of LiFePO$_4$ crystallizing in the olivine-type structure, however, LiMnVO$_4$ is not a good cathode material for rechargeable Li-ion batteries.[8] Recently, the AMnVO$_4$ vanadate series have been extended with AgMnVO$_4$,[9] CuMnVO$_4$,[10] KMnVO$_4$,[11] and RbMnVO$_4$.[9] AgMnVO$_4$ crystallizes in the maricite-type structure and contains MnO_4 chains made up of edge-sharing MnO_6 octahedra. CuMnVO$_4$ crystallizes in the Na_2CrO_4-type structure and also contains MnO_4 chains made up of edge-sharing MnO_6 octahedra. The spin exchange interactions within such MnO_4 chains and between them were found to be antiferromagnetic. Surprisingly, KMnVO$_4$ crystallizes in a new type of oxygen-deficient perovskite, and RbMnVO$_4$ is the first vanadate crystallizing in the stuffed tridymite-type structure.[9]

Toward completing the AMnVO$_4$ series with A = alkali, it is highly desirable to prepare the missing phase NaMnVO$_4$. In the present work, we successfully synthesized this phase, determined its crystal structure by X-ray diffraction, examined its magnetic properties by magnetic susceptibility and specific heat measurements, and analyzed its spin exchange interactions by density functional calculations. Results of our studies are presented in the following section.

*Author to whom correspondence should be addressed. E-mail: benyahia.hamdi@voila.fr.

(1) Geller, S.; Durand, J. L. *Acta Crystallogr.* **1960**, *13*, 325.
(2) Moring, J.; Kostiner, E. *J. Solid State Chem.* **1986**, *61*, 379.
(3) Lujan, M.; Kubel, F.; Schmid, H. *Z. Naturforsch.* **1995**, *50b*, 1210.
(4) Yakubovich, O. V.; Simonov, M. A.; Mel'nikov, O. K. *Kristallografiya* **1990**, *35*, 42.
(5) Ben Yahia, H.; Gaudin, E.; Darriet, J. *J. Alloys Compd.* **2007**, *442*, 74.
(6) Ben Yahia, H.; Gaudin, E.; Darriet, J. *Z. Naturforsch.* **2009**, *64b*, 875.
(7) Padhi, A. K.; Archibald, W. B.; Nanjundaswamy, K. S.; Goodenough, J. B. *Solid State Chem.* **1997**, *128*, 267.
(8) Chung, S.-Y.; Bloking, J. T.; Chiang, Y.-M. *Nat. Mater.* **2002**, *1*, 123.
(9) Ben Yahia, H.; Gaudin, E.; Darriet, J. *J. Solid State Chem.* **2008**, *181*, 3103.
(10) Ben Yahia, H.; Gaudin, E.; Darriet, J.; Banks, M.; Kremer, R. K.; Villesuzanne, A.; Whangbo, M. H. *Inorg. Chem.* **2005**, *44*, 3087.
(11) Ben Yahia, H.; Gaudin, E.; Lee, C.; Whangbo, M. H.; Darriet, J. *Chem. Mater.* **2007**, *19*, 5563.

 Published on Web 08/23/2010

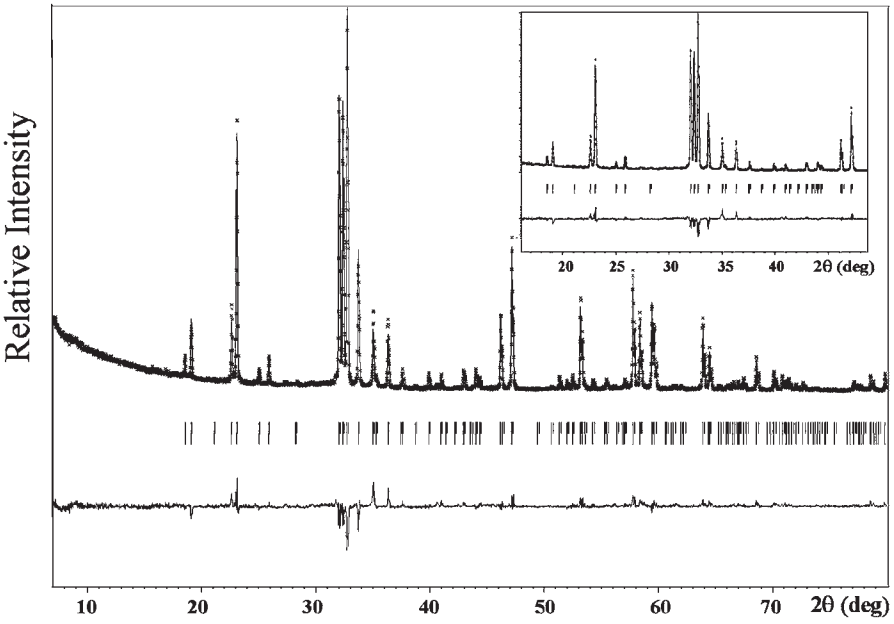

Figure 1. Observed, calculated, and difference plots for the X-ray powder diffraction profile refinement (Cu Kα1−α2 radiation) of $NaMnVO_4$.

2. Experimental Section

Synthesis. Pure $NaMnVO_4$ was prepared by solid state reactions from a stoichiometric mixture of $NaVO_3$ and MnO ($NaVO_3$ was obtained by heating a 1:1 mixture of Na_2CO_3 and V_2O_5 at 600 °C for 6 h). The mixture was put in a gold tube, which was sealed under vacuum in a silica tube, and then heated at 500 °C for 120 h to avoid the melting of $NaVO_3$ (melting point = 610 °C) and at 650 °C for 24 h. After grinding, the mixture is pelletized, fired at 650 °C for 12 h under argon flow, and then quenched in water in order to avoid decomposition of the phase and to clean the sample from traces of $NaVO_3$, which are soluble in water. Single crystals of $NaMnVO_4$ were prepared under vacuum by a fast heating of the pure sample at 950 °C (melting point ≈ 900 °C) and then by slowly decreasing the temperature at the rate of 2 °C h^{-1} to room temperature. The obtained crystals are yellow in color.

Electron Microprobe Analysis. Semiquantitative EPMA analyses of many crystals, including the one investigated on the diffractometer, were carried out with a CAMECA SX-100 instrument. The experimentally observed compositions were close to the compositions obtained from the single crystal refinement. Traces of an impurity with the mean composition of $Na_{3.08}Mn_{0.9}V_{2.02}O_{7.5}$ have been also observed. This indicates a partial decomposition of $NaMnVO_4$. No traces of manganese oxides or $NaVO_3$ have been detected.

Differential Thermal Analysis (DTA). DTA of the $NaMnVO_4$ sample was carried out under argon atmosphere between 25 and 950 °C using a Setaram thermal analyzer at a heating and cooling rate of 5 °C min^{-1}. In a platinum tube, about 60 mg of $NaMnVO_4$ sample was used. From the heating curve, the melting temperature of $NaMnVO_4$ was estimated to be about 900 °C. The two additional transitions observed on the cooling curve might correspond to the melting of binary sodium vanadates (Figure S1 of the Supporting Information).

Powder X-ray Diffraction. To ensure the purity of $NaMnVO_4$ powders, we performed high precision X-ray powder diffraction measurements. The data were collected at room temperature over the 2θ angle range $5° \leq 2\theta \leq 120°$ with a step size of 0.02 or 0.008° using a Philips X-pert diffractometer operating with Cu Kα radiation. Full pattern matching refinements were performed with the Jana2000 program package[12] (Figure 1). The background was estimated by a Legendre function, and the peak shapes were described by a pseudo-Voigt function. The refinement of peak asymmetry was performed using four Berar-Baldinozzi parameters.[13] The diffraction pattern of the powder obtained by melting $NaMnVO_4$ under vacuum has shown an important difference compared to that of the pure $NaMnVO_4$ phase. Most of the diffraction peaks were indexed using $NaMnVO_4$, $Na_3MnV_2O_{7.5}$, and Mn_3O_4 cell parameters (Figure S2 of the Supporting Information). The same powder pattern is obtained after melting the pure sample under Argon atmosphere.

Table 1. Atomic Positions and Isotropic Displacement Parameters for $NaMnVO_4$

atom	sites	*x*	*y*	*z*	U_{eq} (Å^2)
Na	4*c*	0.14622(12)	3/4	0.51349(15)	0.0161(2)
Mn	4*a*	1/2	0	1/2	0.01109(8)
V	4*c*	0.18090(3)	1/4	0.52042(5)	0.00618(7)
O1	4*c*	0.36336(15)	1/4	0.5585(3)	0.0100(3)
O2	4*c*	0.12308(15)	1/4	0.2112(3)	0.0121(4)
O3	8*d*	0.11606(11)	0.44536(16)	0.67228(18)	0.0138(3)

Single Crystal X-ray Diffraction. $NaMnVO_4$ single crystals suitable for single crystal X-ray diffraction were selected on the basis of size and sharpness of the diffraction spots. The data collections were carried out on an Enraf-Nonius Kappa CCD diffractometer using Mo Kα radiation. Data processing and all refinements were performed with the Jana2000 program package.[12] A Gaussian-type absorption correction was applied, and the shape was determined with the video microscope of the Kappa CCD. For the $NaMnVO_4$ data collection details, see Table S1 of the Supporting Information. The extinction conditions observed for single crystal $NaMnVO_4$ agree with the *Pnma* and $Pn2_1a$ space groups. The refinement was performed taking into account the centrosymmetric space group *Pnma*. Most of the atomic positions were found by Direct Methods using Sir97.[14] With anisotropic displacement parameters, the final residual factors converged to the value $R(F) = 0.0304$ and $wR(F^2) = 0.0538$ for 41 refined parameters, 807 observed reflections, and

(12) Petricek, V.; Dusek, M.; Palatinus, L. *Jana2006: The Crystallographic Computing System*; Institute of Physics: Praha, Czech Republic, 2006.

(13) Berar, J. F.; Baldinozzi, G. *J. Appl. Crystallogr.* **1993**, *26*, 128.

(14) Altomare, A.; Burla, M. C.; Camalli, M.; Cascarano, G. L.; Giacovazzo, C.; Guagliardi, A.; Moliterni, A. G. G.; Polidori, G.; Spagna, R. *J. Appl. Crystallogr.* **1999**, *32*, 115.

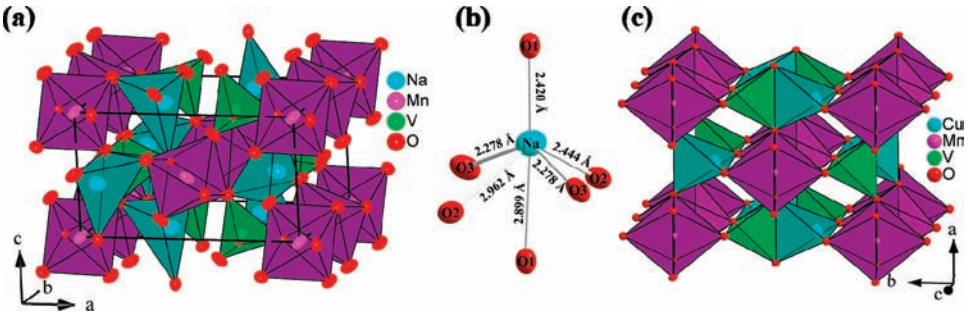

Figure 2. (a) Perspective view of $NaMnVO_4$ structure. (b) Surrounding of sodium atoms. (c) Perspective view of $CuMnVO_4$ structure.

difference-Fourier residues in the range between −1.41 and +1.40 eÅ^{-3}. The Na atoms have a somewhat large anisotropic displacement parameter [U^{11} = 0.0203(5) Å^2]. One might consider this to arise from a partial substitution of Mn for Na. However, the occupancies of all the atoms do not show any significant deviation from the ideal stoichiometric composition. Thus the large anisotropic displacement parameter of Na is due probably to the mobility of the Na atoms. The refined atomic positions and anisotropic displacement parameters (ADPs) are given in Table 1 and Table S2 of the Supporting Information, respectively.

Magnetic Susceptibility and Specific Heat Measurements. Magnetic susceptibility measurements for $NaMnVO_4$ were carried out with a Quantum Design SQUID magnetometer. The susceptibility was recorded at 5 kOe for $NaMnVO_4$ in the whole temperature range 2−300 K. The data were collected during the warm-up cycle at 5 kOe, after the sample was cooled in the zero applied field. The diamagnetic corrections were carried out on the basis of Pascal's tables.[15] Heat capacity measurements were performed on $NaMnVO_4$ pellets using a PPMS Quantum Design in a temperature range from 2 to 100 K.

3. Crystal Structure of $NaMnVO_4$

$NaMnVO_4$ is isostructural with $NaMnPO_4$ of maricite-type structure. The structure consists of edge-sharing chains of MnO_6 octahedra running along the *b* axis. The MnO_6 octahedra are cross connected by the VO_4 tetrahedra, giving rise to large cavities in which the sodium atoms are located (Figures 2a,b). The interatomic distances and the bond valence sum (BVS) are given in Table 2. The Mn−O distances range from 2.099 to 2.368 Å, with an average distance of 2.216 Å. This is very similar to the results found for $NaMnPO_4$,[2] in which the Mn−O distances range from 2.077 to 2.397 Å, with an average distance of 2.229 Å. The BVS of 1.97 is in good agreement with the expected value of +2 for Mn^{2+} (d^5).[16] The vanadium tetrahedron is quite regular with distances ranging from 1.68 to 1.75 Å, with an average value of 1.71 Å. The BVS of 5.08 is in agreement with the expected value of +5 for V^{+5}. The Na^+ ion is bonded to four O atoms belonging to four different MnO_6 groups to form an irregular tetrahedron. The O−Na−O angles range from 87.42(4)° to 124.92(5)°, and the average Na−O distance is 2.355 Å. The BVS is calculated to be 0.92 by using the four shortest Na−O contacts. When the coordination sphere of Na is increased to six (Figure 2b), the BVS becomes 1.016. Thus, the sodium atoms are best considered to be 4 + 2 coordinate (see the Na−O distances listed in Table 2).

Table 2. Interatomic Distances (Å), Bond Valence, and Bond Valence Sum (*BVS) for $NaMnVO_4$

	distances	BVS
Na−O1 (×1)	2.421(2)	0.189
Na−O1 (×1)	2.899(2)	0.052
Na−O2 (×1)	2.963(2)	0.044
Na−O2 (×1)	2.444(2)	0.177
Na−O3 (×2)	2.2784(11)	0.277 (×2)
	<2.355>	*0.92(1) [C.N. = 4]
	<2.547>	*1.01(1) [C.N. = 6]
Mn−O1 (×2)	2.1828(9)	0.346 (×2)
Mn−O2 (×2)	2.3678(10)	0.21 (×2)
Mn−O3 (×2)	2.0995(10)	1.433 (×2)
	<2.216>	*1.97(1) [C.N. = 6]
V−O1 (×1)	1.7565(15)	1.132
V−O2 (×1)	1.7342(14)	1.205
V−O3 (×2)	1.6866(11)	1.372 (×2)
	<1.716>	*5.08(1) [C.N. = 4]

The crystal structures of $NaMnVO_4$ and $CuMnVO_4$ are very similar. Indeed, in these two different structures, the maricite- and the Na_2CrO_4-type, respectively, the cation arrays are similar (Figure 2a,c), but the oxygen arrays are different. This explains the difference in the connectivity between the chains of edge-sharing octahedra and in the other cation coordination polyhedra. The structural transition from the maricite- to the Na_2CrO_4-type structure is possible. Peltier et al. have evidenced this in their studies of α- and β-$InPO_4$ phases.[17] This makes $NaMnVO_4$ and $CuMnVO_4$ strongly related from the structural and magnetic points of view.

4. Magnetic Susceptibility and Specific Heat of $NaMnVO_4$

The plot of the magnetic susceptibility versus temperature (χ vs T) and the corresponding χ^{-1} versus T plot for $NaMnVO_4$ are shown in Figure 3. The χ^{-1} versus T plot reveals that $NaMnVO_4$ exhibits a Curie−Weiss behavior in the temperature range 70 − 300 K, leading to the Curie−Weiss law with θ = −62(1) K and C = 4.31 mol^{-1} cm^3 K. The negative θ indicates that the predominant spin exchange interactions are antiferromagnetic. The effective magnetic moment μ_{eff} calculated from the Curie constant is 5.87(1) μ_B, which is close to the spin only value of 5.92 μ_B expected for a high-spin Mn^{2+} (d^5) ion. The χ versus T plot has a broad maximum (at T_{max} = 24 K), indicating the occurrence of short-range antiferromagnetic order around T_{max} and a local minimum at 11.8 K. The specific heat of $NaMnVO_4$ exhibits a lambda-type anomaly at 11.8 K (Figure 4), which shows that $NaMnVO_4$ undergoes a three-dimensional antiferromagnetic ordering at 11.8 K. Thus, T_{min} corresponds to the

(15) Mabbs, F. E.; Machin, D. J. *Magnetism and Transition Metal Complexes*; Chapman and Hall: London, 1973.
(16) Brown, I. D.; Altermatt, D. *Acta Crystallogr., Sect. B: Struct. Sci.* **1985**, *41*, 244.
(17) Peltier, V.; Deniard, P.; Brec, R.; Marchand, R. *C. R. Acad. Sci., Ser. II* **1998**, *1*, 57.

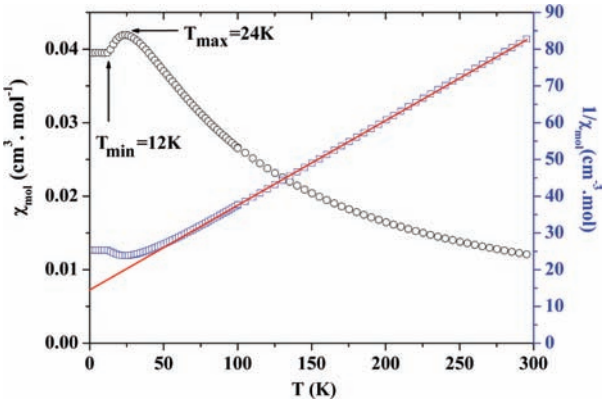

Figure 3. Magnetic susceptibility χ vs temperature and the corresponding χ^{-1} vs T plots of $NaMnVO_4$ measured in the applied field H = 5 kOe.

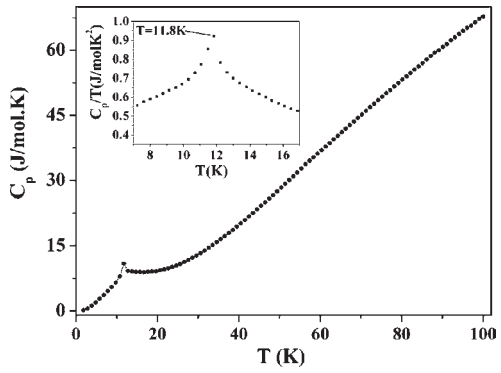

Figure 4. Specific heat C_p vs T plot of $NaMnVO_4$. The inset displays C_p/T in the region of the magnetic transition at 11.8 K.

Néel temperature T_N = 11.8 K. It is noted that $CuMnVO_4$ has the same type of edge-sharing MnO_4 chains (Figure 2c) and exhibits a similar magnetic behavior with T_{max} = 28 K and T_{min} = T_N = 20 K.[10]

Given that $\theta = -62$ K and T_N = 11.8 K, the spin exchanges of $NaMnVO_4$ are frustrated ($|\theta|/T_N > 5$).[18] We fitted the magnetic susceptibility curve of $NaMnVO_4$ above T_N in terms of the interacting uniform chain model (with the intra- and interchain spin exchanges J_{intra} and J_{inter}, respectively), as carried out for $CuMnVO_4$ in ref 10, without considering the contribution of paramagnetic impurities. This fitting analysis leads to a very good agreement between the calculated and experimental susceptibilities. Unlike the case of $CuMnVO_4$ ($J_{inter}/J_{intra} \approx 0.29$),[10] but J_{inter} is found to be comparable in magnitude to J_{intra} for $NaMnVO_4$ (i.e., $J_{inter}/J_{intra} \approx 1$). Thus, the use of the interacting uniform chain model is not appropriate for $NaMnVO_4$ because it requires that $J_{inter}/J_{intra} \ll 1$. Therefore, we attempted to fit the magnetic susceptibility data using a classical antiferromagnetic Heisenberg chain with spin S = 5/2 and intrachain exchange J_{intra} (see eq 2 in ref 10), but this model does not adequately describe the data. This is most probably because of the presence of significant interchain exchange interactions (see below).

5. Spin Exchange Interactions

In $NaMnVO_4$, only the high-spin Mn^{2+} (S = 5/2) ions are magnetic ions. As depicted in panels a and b of Figure 5, we consider the four spin-exchanges J_1−J_4 between the Mn^{2+} ions; J_1 is the Mn−O−Mn superexchange between adjacent Mn^{2+} ions along each edge-sharing MnO_4 chain along the b-direction, while J_2−J_4 are Mn−O···O−Mn supersuperexchanges between adjacent MnO_4 chains, which are mediated by VO_4 units. It should be noted that a Mn^{2+} site of each MnO_4 chain gives rise to four J_3 exchanges with the neighboring MnO_4 chains as depicted in Figure 5b. The Mn···Mn and O···O distances associated with these spin exchanges are summarized in Table 3. To determine the values of these exchanges, we first examine the five ordered spin states, defined in Figure 6 in terms of a (a, b, 2c) supercell containing eight formula units (FUs). The total spin exchange energies of these states can be expressed in terms of the spin Hamiltonian $\hat{H} = -\sum_{i<j} J_{ij}\hat{S}_i \times \hat{S}_j$, where $J_{ij} = J_1 - J_4$. By applying the energy expressions obtained for spin dimers with N unpaired spins per spin site (in the present case, N = 5),[19] the total spin exchange energies (per 4 FUs, i.e., per one chemical unit cell) of the five ordered spin states are written as

$$\begin{aligned}
&\text{FM}: (-4J_1 - 8J_2 - 8J_3 - 4J_4)(N^2/4)\\
&\text{AF1}: (+4J_1 - 8J_2 + 8J_3 - 4J_4)(N^2/4)\\
&\text{AF2}: (+4J_1 + 8J_2 - 8J_3 - 4J_4)(N^2/4)\\
&\text{AF3}: (-4J_1 + 8J_2 + 8J_3 - 4J_4)(N^2/4)\\
&\text{AF4}: (+4J_3)(N^2/4)
\end{aligned} \quad (1)$$

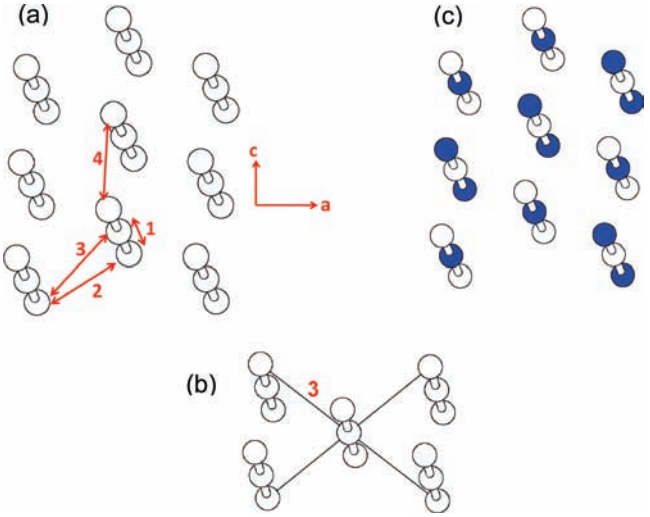

Figure 5. (a) Schematic representation of the spin exchange paths J_1−J_4 in $NaMnVO_4$, where the circles represent the Mn^{2+} (S = 5/2) spin sites while the numbers 1−4 represent J_1 − J_4, respectively. The J_1 magnetic bonds along the b-direction are represented by the cylinders. (b) The occurrence of four spin exchanges J_3 at a given Mn^{2+} site. (c) The magetic structure of the magnetic ground state expected below T_N, where the unshaded and shaded circles represent the Mn^{2+} ions with up-spin and down-spin, respectively.

Table 3. Geometrical Parameters Associated with Spin Exchanges J_1−J_4 in $NaMnVO_4$ and Values of J_1−J_4 Determined from GGA+U Calculations

	distance (Å)		J/k_B (K)	
exchange	Mn···Mn	O···O	U = 4 eV	U = 5 eV
J_1	3.441[a]		−6.13	−4.84
J_2	5.471	2.787	−0.64	−0.51
J_3	6.463	2.787	−0.52	−0.41
J_4	5.316	2.975	−1.25	−1.00

[a] The ∠Mn−O−Mn = 104.04°.

(18) (a) Greedan, J. E. *J. Mater. Chem.* **2001**, *11*, 37. (b) Dai, D.; Whangbo, M.-H. *J. Chem. Phys.* **2004**, *121*, 672.

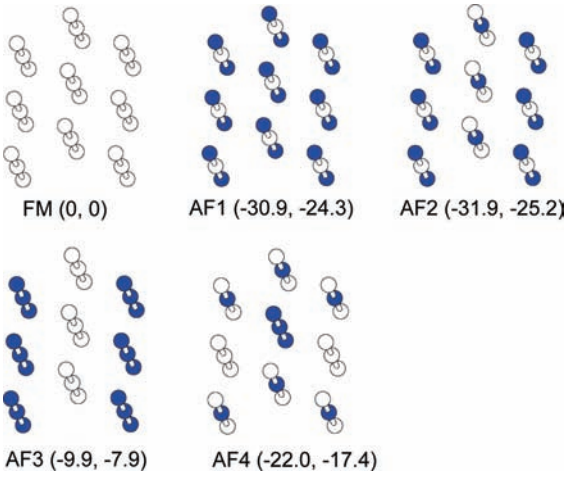

Figure 6. Five ordered spin states of $NaMnVO_4$ employed to extract the spin exchanges J_1-J_4 by using a (a, b, 2c) supercell. The unshaded and shaded circles represent the Mn^{2+} ions with up-spin and down-spin, respectively. The two numbers in the parentheses (from left to right) for each state are the relative energies (in meV per 4 FUs) obtained from the GGA+U calculations (with $U = 4$ and 5 eV, respectively).

To determine the values of J_1-J_4, we determine the relative energies of the five ordered spin states on the basis of density functional calculations. Our calculations employed the frozen-core projector augmented wave method[20] encoded in the Vienna ab initio simulation packages[21] and the generalized-gradient approximation (GGA)[22] with the plane-wave-cutoff energy of 500 eV and a set of 36 k points for the irreducible Brillouin zone. To properly describe the effect of electron correlation in the Mn 3d states, the GGA plus on-site repulsion method (GGA+U)[23] was used with the effective U values of 4 and 5 eV. The relative energies (per 4 FUs) of the five ordered spin states obtained from GGA+U calculations are summarized in Figure 6. Thus, by mapping the relative energies of the five spin ordered states onto the corresponding energies expected from the total spin exchange energies listed in eq 1, we obtain the values of J_1-J_4 summarized in Table 3.

To see how reasonable the extracted spin exchanges are, we calculate the Curie−Weiss temperature θ, which in the mean field theory[24] is related to spin exchanges as

$$\theta = \frac{S(S+1)}{3k_B}\sum_i z_i J_i \qquad (2)$$

where the summation runs over all nearest neighbors of a given spin site, z_i is the number of nearest neighbors connected by the spin exchange parameter J_i, and S is the spin quantum number of each spin site (i.e., $S = 5/2$ in the present case). Thus, for $NaMnVO_4$, θ can be approximated by

$$\theta \approx \frac{35(2J_1 + 4J_2 + 4J_3 + 2J_4)}{12k_B} \qquad (3)$$

The θ value is estimated to be −56.6 and −44.8 by using the spin exchange parameters from the GGA+U calculations with $U = 4$ and 5 eV, respectively. This is in good agreement with experiment (i.e., −62 K), given that GGA+U electronic structure calculations generally overestimate the magnitude of spin exchange interactions by a factor approximately up to four.[25]

In $NaMnVO_4$, the intrachain exchange J_1 is by far the strongest exchange, which forms uniform antiferromagnetic chains along the b-direction. This explains the occurrence of a broad maximum in the magnetic susceptibility at 24 K. The spin exchanges J_1-J_4 are all antiferromagnetic. Therefore, the exchanges in the (J_1, J_2, J_3) and (J_2, J_2, J_4) triangles are spin-frustrated (Figure 5a,b), namely, the interchain spin exchanges are spin-frustrated. This explains why T_N is considerably smaller than $|\theta|$ in $NaMnVO_4$ (11.8 vs 62 K). It is of interest to consider the probable magnetic structure for the ordered antiferromagnetic state below T_N. Among the interchain spin exchanges, J_4 is stronger than J_2 and J_3 by a factor of ∼2. Thus, the magnetic structure shown in Figure 5c, in which the spins are antiferromagnetically coupled in all J_1 and J_4 magnetic bonds, is energetically most favorable and hence is expected to represent the ordered magnetic structure of $NaMnVO_4$ below T_N.

6. Concluding remarks

$NaMnVO_4$ crystallizes in the maricite-type structure as does $NaMnPO_4$ and undergoes a three-dimensional antiferromagnetic ordering at $T_N = 11.8$ K, with a broad maximum in the magnetic susceptibility at $T_{max} = 24$ K. The broad maximum reflects the fact that the strongest spin exchange J_1 forms uniform antiferromagnetic chains, and T_N is considerably smaller in magnitude than the Curie−Weiss temperature of −62 K because the interchain spin exchanges are spin-frustrated. Our study predicts that, in the ordered magnetic structure below T_N, the spins are antiferromagnetically coupled in all J_1 and J_4 magnetic bonds. It would be interesting to verify this prediction by neutron diffraction measurements.

Acknowledgment. The authors acknowledge the work that occurred at NCSU funded by the Office of Basic Energy Sciences, Division of Materials Sciences, U.S. Department of Energy, under Grant DE-FG02-86ER45259, and also the computing resources of the NERSC center and the HPC center of NCSU.

Supporting Information Available: X-ray diffraction details (CIF) as well as Tables S1 and S2 and Figures S1 and S2. This material is available free of charge via the Internet at http://pubs.acs.org.

(19) (a) Dai, D.; Whangbo, M.-H. *J. Chem. Phys.* **2001**, *114*, 2887. (b) Dai, D.; Whangbo, M.-H. *J. Chem. Phys.* **2003**, *118*, 29.
(20) Blöchl, P. E. *Phys. Rev. B* **1994**, *50*, 17953.
(21) (a) Kresse, G.; Hafner, J. *Phys. Rev. B* **1993**, *47*, 558. (b) Kresse, G.; Furthmüller, J. *Comput. Mater. Sci.* **1996**, *6*, 15. (c) Kresse, G.; Furthmüller, J. *Phys. Rev. B* **1996**, *54*, 11169.
(22) Perdew, J. P.; Burke, K.; Ernzerhof, M. *Phys. Rev. Lett.* **1996**, *77*, 3865.
(23) Dudarev, S. L.; Botton, G. A.; Savrasov, S. Y.; Humphreys, C. J.; Sutton, A. P. *Phys. Rev. B* **1998**, *57*, 1505.
(24) Smart, J. S. *Effective Field Theory of Magnetism*; Saunders: Philadelphia, 1966.
(25) (a) Xiang, H. J.; Lee, C.; Whangbo, M.-H. *Phys. Rev. B: Rapid Commun* **2007**, *76*, 220411(R). (b) Koo, H.-J.; Whangbo, M.-H. *Inorg. Chem.* **2008**, *47*, 128. (c) Koo, H.-J.; Whangbo, M.-H. *Inorg. Chem.* **2008**, *47*, 4779.